AIAA JOURNAL
Vol. 47, No. 2, February 2009

Effective Far-Field Acoustic Prediction Method and its Computational Aeroacoustics Applications

Chao Yu,* Zhengfang Zhou,† and Mei Zhuang‡
Michigan State University, East Lansing, Michigan 48823
Xiaodong Li§
Beihang University, 100083 Beijing, People's Republic of China
and
Frank Thiele¶
Technical University of Berlin, 10623 Berlin, Germany

DOI: 10.2514/1.39009

A three-dimensional acoustic intensity-based method for the reconstruction and prediction of radiated acoustic fields is developed. The method is verified by examples of the propagation of multiple acoustic sources in a uniform flow and the acoustic scattering of a time-dependent source by a sphere. The effectiveness of acoustic intensity-based method in aeroacoustic applications is demonstrated by the accurate and efficient prediction of acoustic radiation from an axisymmetric duct intake using a hybrid computational aeroacoustics/acoustic intensity-based method approach. The results of the radiated acoustic field from the acoustic intensity-based method agree well with the solutions of computational aeroacoustics and the Ffowcs Williams–Hawkings integral equation. The acoustic intensity-based method is more efficient than other methods for the far-field acoustic prediction and can use the input acoustic data from an open surface instead of a closed surface, such as the Ffowcs Williams–Hawkings surface.

Nomenclature

A_0	=	acoustic source strength
c	=	speed of sound
G_n	=	n-th order generalized Hankel function of the second kind
i	=	$\sqrt{-1}$
k	=	wave number, ω/c
M	=	number of input locations
M_a	=	freestream Mach number
$\mathbf{n}$	=	unit normal vector, (n_x, n_y, n_z)
P	=	acoustic pressure in the frequency domain
p	=	acoustic pressure in the time domain
p_j	=	acoustic pressure from a monopole sound source
P_N	=	approximated acoustic pressure in the frequency-domain
P_n^m	=	associated Legendre polynomial
r, θ, ϕ	=	spherical coordinates
$\hat{r}, \hat{\theta}, \hat{\phi}$	=	modified spherical coordinates
t	=	time
$\mathbf{U}$	=	freestream velocity vector, (U, V, W)
x, y, z	=	Cartesian coordinates
$\hat{x}, \hat{y}, \hat{z}$	=	modified Cartesian coordinates
β	=	$\sqrt{1 - M_a^2}$
Γ	=	spherical boundary containing all the acoustic sources
Γ_1	=	partial boundary of Γ
ρ_0	=	freestream density
Φ	=	velocity potential function
ω	=	angular frequency

Presented as Paper 3053 at the 14th AIAA/CEAS Aeroacoustics Conference (29th AIAA Aeroacoustics Conference), Vancouver British Columbia, 5–7 May 2008; received 9 June 2008; accepted for publication 13 October 2008.

*Graduate Student, Department of Mechanical Engineering. Member AIAA.
†Professor, Department of Mathematics.
‡Associate Professor, Department of Mechanical Engineering; currently Professor, Aerospace Engineering Department, The Ohio State University. Associate Fellow AIAA.
§Professor, School of Jet Propulsion. Associate Fellow AIAA.
¶Professor, Hermann Foettinger Institute for Fluid Mechanics, Strasse des 17, Juni 135, D-10623.

I. Introduction

ONE of the biggest problems posed by the expansion of air travel is its noise impact on communities. Aircraft noise prediction and control thus become one of the most urgent and challenging tasks. A hybrid approach is usually considered for predicting aerodynamic noise. The approach separates the field into aerodynamic source and acoustic propagation regions. Conventional computational fluid dynamics (CFD) solvers are typically used to evaluate the flowfield solution in the near field to provide the aerodynamic sound source. Once the sound source is predicted, the linearized Euler equations (LEE) or integral methods based on Lighthill's analogy [1] are used for the prediction of the acoustic wave propagation. The LEE methods assume the flowfield to be a time-averaged mean flow and a time-dependent small disturbance. The extension of the near-field CFD solution to the midfield acoustic radiation can be achieved using the LEE methods. However, the evaluation of the far-field radiation is prohibited by excessive computer memory requirements. As an alternative, the integral methods, for example the Kirchhoff method [2] and the permeable surface Ffowcs Williams–Hawkings (FW–H) equation method [3], are commonly used to predict the far-field radiating sound using the flowfield quantities on a closed control surface (that encloses the entire aerodynamic source region) if the wave equation is assumed outside. The surface integration, however, has to be carried out for each far-field location. This would be still computationally intensive for a practical three-dimensional problem even though the intensity in terms of the CPU time has been much decreased compared with that required by the LEE methods. For an accurate far-field prediction, the other difficulty of using these integral methods for some aeroacoustic problems is that the control surface must completely enclose the aerodynamic source region. This may be infeasible or impossible to accomplish for some practical cases.

Motivated by the need for an accurate and efficient prediction of the far-field acoustic radiation, an acoustic intensity-based method

(AIBM) has been developed based on acoustic input from an open control surface in a two-dimensional configuration [4,5]. Like the Kirchhoff method, the AIBM assumes that the sound propagation is governed by the simple Helmholtz equation in the frequency domain on and outside a control surface that encloses all the nonlinear effects and noise sources. The prediction of the acoustic radiation field is, however, carried out with an input of the acoustic pressure derivative and its simultaneous, colocated acoustic pressure over an open control surface. The reconstructed acoustic radiation field using the AIBM is unique due to the unique continuation theory of elliptic equations [6]. Hence, the method is more stable, and the predicted acoustic pressure is less dependent on the locations of the input acoustic data [4]. The input acoustic data can be provided from results of the near-field CFD/CAA (computational aeroacoustics) or experimental measurements in a radiated acoustic field.

In this paper, the details on the extension of AIBM to a three-dimensional configuration with a subsonic uniform flow are given. The accuracy of AIBM for the acoustic far-field prediction is shown by numerical examples, and the advantages of the method with respect to both efficiency and choice of acoustic input locations are demonstrated.

II. Mathematical Formulations

Let Γ be the boundary of a sphere containing all acoustic sources, and Γ_1 be a (usually very small) part of Γ. In the AIBM, both the acoustic pressure P and its collocated normal derivative $\partial P/\partial \mathbf{n}$ on Γ_1 are considered as the input acoustic data. In practice, P and $\partial P/\partial \mathbf{n}$ are given at a finite number of points $(x_j, y_j, z_j) \in \Gamma_1$, $j = 1, M$.

A. Basic Formulation for AIBM

Assuming that the mean flow is in z direction and employing the standard separation of variables in terms of spherical coordinates, the general solution for the Helmholtz equation can be approximated by a linear combination of basis functions

$$P(r,\theta,\phi) = \exp(ikM_a\hat{r}\cos\hat{\phi}\beta^{-2}) \times \sum_{n=0}^{\infty}\sum_{m=0}^{n}(a_{nm}\cos m\hat{\theta} + b_{nm}\sin m\hat{\theta})P_n^m(\cos\hat{\phi})G_n(k\hat{r}\beta^{-2}) \quad (1)$$

The coordinates $(\hat{r}, \hat{\theta}, \hat{\phi})$ are defined as the modified spherical coordinates from Cartesian coordinates (x, y, z) in the physical domain. Let $(\hat{x}, \hat{y}, \hat{z}) = (\beta x, \beta y, z)$, then

$$\hat{x} = \hat{r}\sin\hat{\phi}\cos\hat{\theta}, \quad \hat{y} = \hat{r}\sin\hat{\phi}\sin\hat{\theta}, \quad \hat{z} = \hat{r}\cos\hat{\phi}, \quad \hat{r} = \sqrt{\hat{x}^2+\hat{y}^2+\hat{z}^2} \quad (2)$$

Differentiating both sides of Eq. (1) with respect to the unit normal $\mathbf{n} = (n_x, n_y, n_z)$ and using the chain rule, we have the formula for the normal derivative of P

$$\frac{\partial P}{\partial \mathbf{n}}(r,\theta,\phi) = \frac{\partial P}{\partial \hat{r}}\frac{\partial \hat{r}}{\partial \mathbf{n}} + \frac{\partial P}{\partial \hat{\theta}}\frac{\partial \hat{\theta}}{\partial \mathbf{n}} + \frac{\partial P}{\partial \hat{\phi}}\frac{\partial \hat{\phi}}{\partial \mathbf{n}} \quad (3)$$

Note that

$$\frac{\partial \hat{\theta}}{\partial \mathbf{n}} = \frac{1}{\hat{r}\sin\hat{\phi}\cos\hat{\theta}}\left(\beta n_y - \hat{r}\cos\hat{\phi}\sin\hat{\theta}\frac{\partial\hat{\phi}}{\partial \mathbf{n}} - \sin\hat{\phi}\sin\hat{\theta}\frac{\partial\hat{r}}{\partial \mathbf{n}}\right) \quad (4)$$

and

$$\frac{\partial \hat{\phi}}{\partial \mathbf{n}} = \frac{1}{\hat{r}\sin\hat{\phi}}\left(\cos\hat{\phi}\frac{\partial\hat{r}}{\partial \mathbf{n}} - n_z\right) \quad (5)$$

As it is shown in the preceding two equations, there are singularities when $\hat{\phi} = 0$ and π or $\hat{\theta} = \pi/2$ and $3\pi/2$. These singularities lead to computational difficulties. To eliminate these poles, an improved formulation is derived in the next section.

B. Improved Formulation for AIBM

In this section, the coordinate system will be converted from spherical coordinates to Cartesian coordinates, and the singularity terms will be eliminated after the multiplication of suitable trigonometric functions.

First, $\cos m\hat{\theta}$ and $\sin m\hat{\theta}$ can be expressed as

$$\begin{cases} \cos m\hat{\theta} = \frac{1}{2}(e^{im\hat{\theta}} + e^{-im\hat{\theta}}) = \frac{1}{2\hat{r}^m\sin^m\hat{\phi}}[(\hat{x}+i\hat{y})^m + (\hat{x}-i\hat{y})^m], \\ \sin m\hat{\theta} = \frac{1}{2i}(e^{im\hat{\theta}} - e^{-im\hat{\theta}}) = \frac{1}{2i\hat{r}^m\sin^m\hat{\phi}}[(\hat{x}+i\hat{y})^m - (\hat{x}-i\hat{y})^m] \end{cases} \quad (6)$$

Substituting the preceding equations into Eq. (1), we have

$$P(x,y,z) = \exp(ikM_a\hat{z}\beta^{-2}) \times \sum_{n=0}^{\infty}\sum_{m=0}^{n}[a_{nm}\xi_m - ib_{nm}\eta_m]Q_n^m(\hat{z}\hat{r}^{-1})G_n(k\hat{r}\beta^{-2})/(2\hat{r}^m) \quad (7)$$

where

$$\xi_m = (\hat{x}+i\hat{y})^m + (\hat{x}-i\hat{y})^m, \qquad \eta_m = (\hat{x}+i\hat{y})^m - (\hat{x}-i\hat{y})^m \quad (8)$$

and $Q_n^m = P_n^m/\sin^m\hat{\phi}$. From the expression for P_n^m, we note that

$$Q_n^m(w) = \frac{(-1)^{m+n}}{2^n n!}\frac{\mathrm{d}^{n+n}}{\mathrm{d}w^{n+m}}(1-w^2)^n|_{w=\hat{z}/\hat{r}}$$

which has no singularity. Therefore, Eq. (7) is an improved form of the general solution of the Helmholtz equation. The corresponding normal pressure derivative can be derived as

$$\frac{\partial P}{\partial \mathbf{n}}(x,y,z) = \frac{\partial P}{\partial \hat{x}}\beta n_x + \frac{\partial P}{\partial \hat{y}}\beta n_y + \frac{\partial P}{\partial \hat{z}}n_z \quad (9)$$

C. Simplified 2.5-D Formulation for AIBM

Axisymmetric problems are sometimes considered as 2.5-D problems (e.g., acoustic modes propagation in an axisymmetric duct intake with an axisymmetric mean flow). In this section, we are going to simplify the 3-D improved formulation into a 2.5-D formulation. Let m be the azimuthal mode and assume that the mean flow is along the z direction. If θ is specified in Eq. (7), for example $\theta = 0$ ($\xi_m = 2\hat{x}^m$, $\eta_m = 0$), the equation can be simplified on the $x-z$ plane as

$$P(x,0,z) = \exp(ikM_a\hat{z}\beta^{-2})\sum_{n=0}^{\infty}\sum_{m=0}^{n}a_{nm}\hat{x}^m Q_n^m(\hat{z}\hat{r}^{-1})G_n(k\hat{r}\beta^{-2})/\hat{r}^m \quad (10)$$

Especially if the mode m is known in advance, the formula can be further simplified as

$$P(x,0,z) = \exp(ikM_a\hat{z}\beta^{-2})\sum_{n=m}^{\infty}a_{nm}\hat{x}^m Q_n^m(\hat{z}\hat{r}^{-1})G_n(k\hat{r}\beta^{-2})/\hat{r}^m \quad (11)$$

This is the simplified 2.5-D solution of the Helmholtz equation for axisymmetric propagation problems. The normal derivative can be derived based on the preceding simplified solution as

$$\frac{\partial P}{\partial \mathbf{n}}(x,0,z) = \frac{\partial P}{\partial \hat{x}}\beta n_x + \frac{\partial P}{\partial \hat{z}}n_z \quad (12)$$

D. Numerical Implementation

The numerical solutions for Eqs. (1), (7), (10), and (11) are obtained from the following three steps:

1) Instead of using the infinite summation in these equations, the solutions are approximated by a finite summation. Namely, the size of n is suitably restricted. For example, Eq. (7) is approximated by

$$P_N = \exp(ikM_a\hat{z}\beta^{-2}) \times \sum_{n=0}^{N}\sum_{m=0}^{n}[a_{nm}\xi_m - ib_{nm}\eta_m]Q_n^m(\hat{z}\hat{r}^{-1})G_n(k\hat{r}\beta^{-2})/(2\hat{r}^m) \quad (13)$$

The upper limit N must be chosen large enough to accurately reconstruct the acoustic data both on the input surface and in the radiated field, but the number should be minimized to reduce the computational costs. N is initialized within a given range $1 \le N \le 20$. The optimum N is determined from the minimum overall error [4].

2) The coefficients a_{nm} and b_{nm}, where $0 \le m \le n \le N$, are numerically determined by matching the assumed form of the solution to the input data $P(x_j, y_j, z_j)$ and $\partial P(x_j, y_j, z_j)/\partial \mathbf{n}$, where $1 \le j \le M$. Namely, a linear system of $2M$ equations with a_{nm} and b_{nm} as unknowns must be solved. One obvious requirement is that this system must be overdetermined, which also restricts the size of N. In the paper, the least-squares method is used to solve this linear system.

3) For any given field point, including the input points, in a radiated acoustic field, the acoustic pressure can be approximated by Eq. (13) using the coefficients a_{nm} and b_{nm} obtained from the previous steps. Detailed numerical techniques are described in the earlier publications [4,5].

III. Results and Discussions

A. Multiple Sources in a Uniform Flow

To verify the accuracy of AIBM in a three-dimensional configuration, acoustic radiation of multiple sources in a uniform flow are studied. A schematic diagram of the sources and their locations is shown in Fig. 1. The mean flow is in the x direction with a Mach number of 0.5. The density and the speed of sound of the ambient medium are given as 1.21 kg/m^3 and 344 m/s, respectively. All the multiple sources radiate with the same angular frequency $\omega = 200$ Hz. The analytical solution for the multiple sources can be obtained by the summation of each point source solution as

$$p(t, x, y, z) = \sum_{j=1}^{J} p_j(t, x, y, z) \quad (14)$$

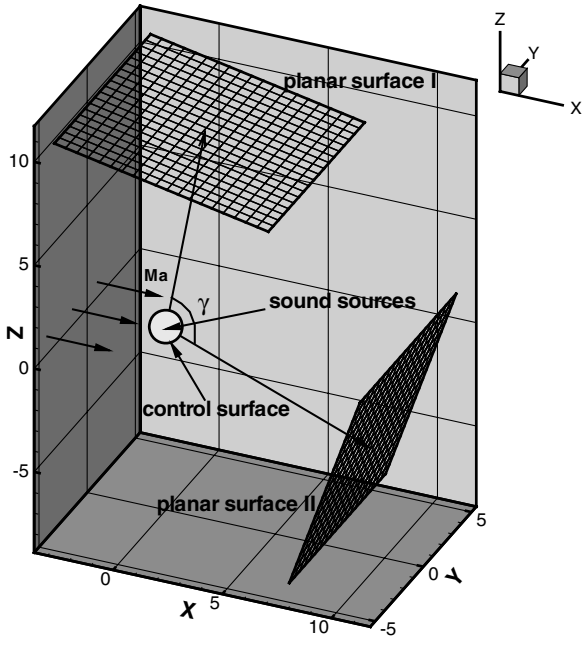

Fig. 1 Schematic diagram of multiple sources in a uniform flow.

Table 1 The strengths and distributions of the acoustic sources

	$A_0, W/m^2$	x, m	y, m	z, m
Quadrupole I	1.0	0.0	−0.5	0.5
	−1.0	0.0	0.5	0.5
	1.0	0.0	0.5	−0.5
	−1.0	0.0	−0.5	−0.5
Quadrupole II	0.8	−0.6	0.0	0.6
	−0.8	0.6	0.0	0.6
	0.8	0.6	0.0	−0.6
	−0.8	−0.6	0.0	−0.6
Dipole I	1.1	0.4	0.3	0.1
	−1.1	0.7	−0.1	0.5
Dipole II	0.9	0.3	0.2	−0.2
	−0.9	−0.2	0.5	−0.3
Monopole	1.0	−0.5	−0.5	−0.1

where p is the acoustic pressure of the radiated field from the multiple sources and p_j is the solution of each point source. The analytical solution of a monopole in a uniform flow is given as [7]

$$p_j = -\rho_0\left(\frac{\partial \Phi}{\partial t} + U\frac{\partial \Phi}{\partial x}\right) \quad (15)$$

with Φ, the velocity potential function, expressed as

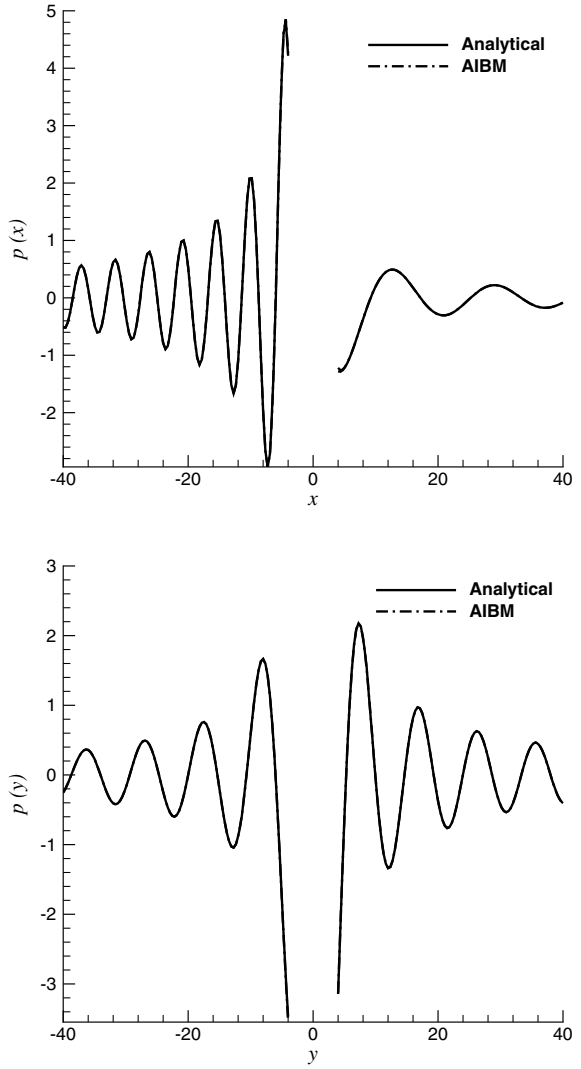

Fig. 2 Comparisons of the predicted pressure solutions with the analytical solutions, shown along the x axis (top) and along the y axis (bottom).

$$\Phi(t,x,y,z)=\frac{A_0}{4\pi\hat{r}}\exp[i(\omega t-k(\hat{r}-M_a x)\beta^{-2})] \qquad (16)$$

where $\beta=\sqrt{1-M_a^2}$, $\hat{r}=\sqrt{x^2+\beta^2(y^2+z^2)}$, and A_0, ω are the strength and the angular frequency of the monopole, respectively.

In the current study, the multiple sources, consisting of two quadrupoles, two dipoles (formed by superposing monopoles), and one monopole, are distributed inside a control surface of $r=1$ m. The coordinates and strengths of the sources are given in Table 1.

The acoustic pressure and its normal derivative on the two planar surfaces are considered as the input for AIBM (see Fig. 1) and obtained by using the fast fourier transformation of the analytical solution of Eq. (14). In the current implementation, the distance of each planar surface to the origin is given as 10 m, and the size of the each surface is 4 by 4 m. The angle γ between the surfaces is 120 deg. Each surface was discretized into 10 by 10 uniform grid lines. The radiated acoustic field for the range of 4 m $\leq r \leq$ 40 m is then predicted by AIBM.

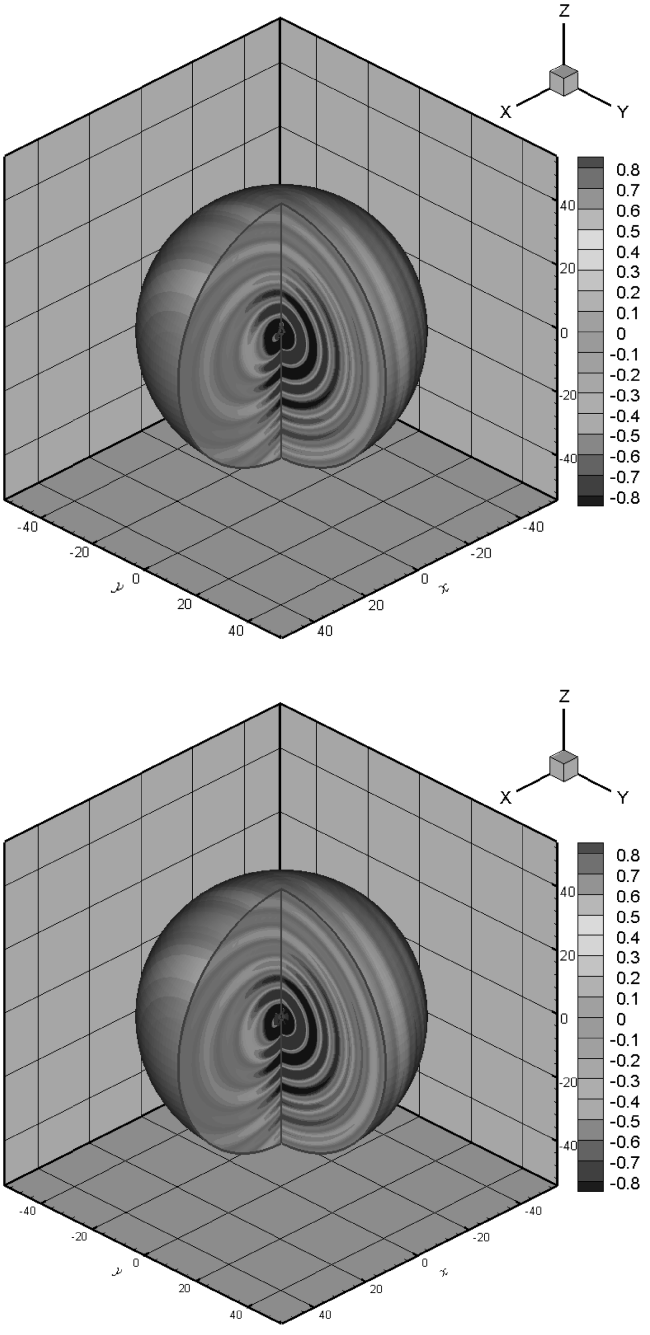

Fig. 3 3-D instantaneous pressure contours for the sound radiation of multiple sources, showing analytical (top) and AIBM (bottom).

Quantitative comparisons of the predicted pressure with the analytical pressure are shown in Fig. 2 along the x axis and the y axis. Excellent agreement of the radiated pressure solutions from the near field to the far field is demonstrated in the figure. Contours of the

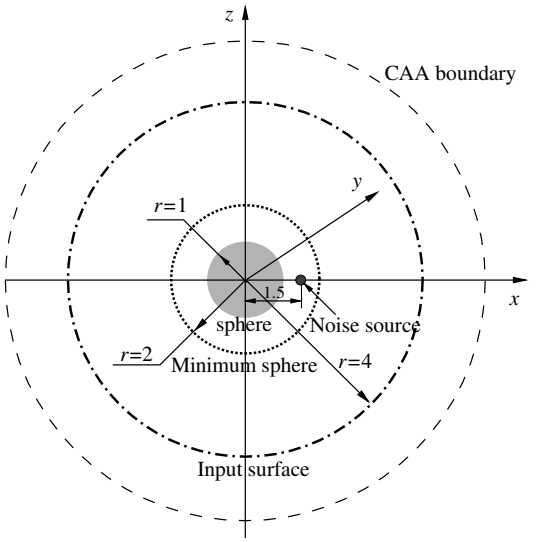

Fig. 4 Schematic diagram of acoustic scattering by a sphere.

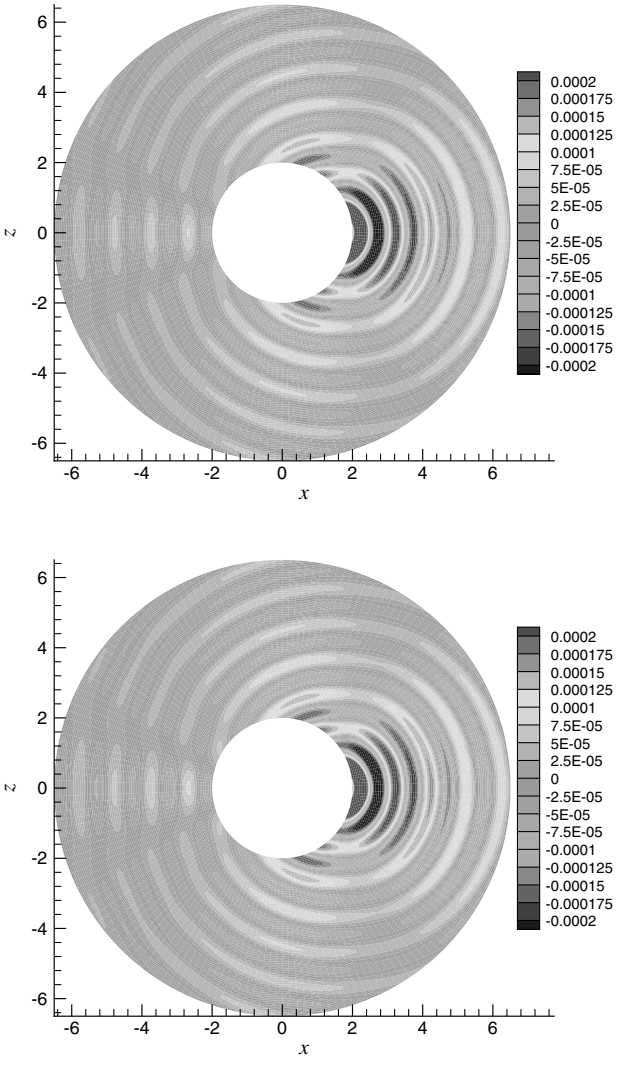

Fig. 5 Instantaneous pressure contours of the sound scattering in the plane $y=0$ showing CAA (top) and AIBM (bottom).

instantaneous pressure are compared with the respective analytical solutions in Fig. 3. These pressure contour results substantiate that AIBM accurately predicts the radiated acoustic field in a uniform flow of a three-dimensional configuration.

B. Acoustic Scattering

This example is an ideal model of the physical problem of predicting the sound field generated by a propeller scattered by the fuselage of a moving aircraft. In the model, the fuselage is considered as a sphere and the noise source (propeller) as a time-dependent, single-frequency acoustic source. The mean flow is given as a Mach number of zero. The dimensionless radius of the sphere is given as 1. The Cartesian coordinates centered at the center of the sphere are shown in Fig. 4. The governing equations for this problem are the linearized Euler equations. The acoustic source is located on the x axis at $x = 1.5$ and expressed as

$$S = 0.01 \exp[-16 \ell_n 2((x-1.5)^2 + y^2 + z^2)] \cos(2\pi t) \qquad (17)$$

The CAA solution [8] verified by the analytical solution of the scattering by a sphere [9] was used as the acoustic input for AIBM calculations. The input surface of $r = \sqrt{x^2 + y^2 + z^2} = 4$ is also depicted in Fig. 4. It is worth mentioning that the input surface for AIBM can be an open surface as indicated in the previous example. Because the CPU time is not at all an issue here, a spherical surface was used for the sake of simplicity.

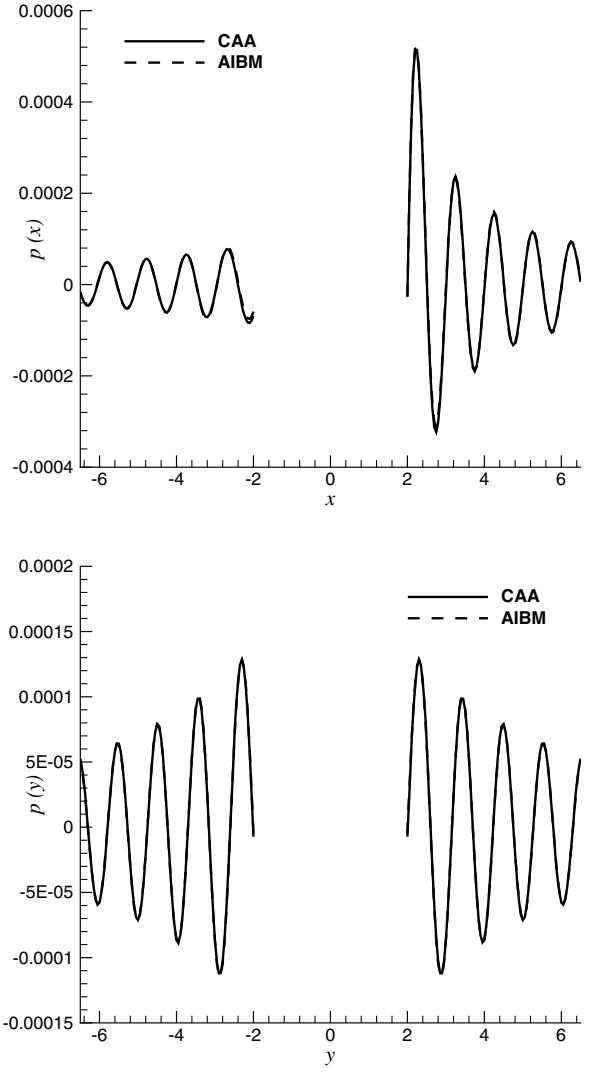

Fig. 6 Comparisons of the predicted pressure solutions with the CAA solutions, shown along the x axis (top) and along the y axis (bottom).

The predicted instantaneous pressure contours by AIBM are compared with the CAA solution in Fig. 5 for the plane of $y = 0$. As it is noted from the figure, the predicted radiated acoustic field agrees very well with the CAA solutions outside a minimum sphere ($r = 2$) that encloses the acoustic sources. The proper size of a minimum sphere was discussed in our previous work [4]. Quantitative comparisons of the perturbation pressure along the x axis and the y axis are shown in Fig. 6. Again an excellent agreement is achieved.

C. Acoustic Propagation and Radiation from an Axisymmetric Duct Intake

Both CAA methods [10–12] and the FW–H integral method coupled with CAA methods [13] were used in the past for the prediction of acoustic propagation and radiation from an engine inlet. In the current study, an axisymmetric geometric model of a duct intake is considered with a uniform subsonic flow. Small acoustic perturbations are propagating upstream through the axisymmetric duct flow and radiating to the far field. A schematic of the duct intake configuration along with the Cartesian and the spherical coordinates and the domain of acoustic propagation and radiation is shown in Fig. 7. The far-field flow pressure, density, Mach number, and the speed of sound are given as $P_\infty = 101.325$ kPa, $\rho_\infty = 1.249$ kg/m^3, $M_{a\infty} = 0.19$ (in negative z direction), and $c_\infty = 337$ m/s, respectively. A single frequency sound source with

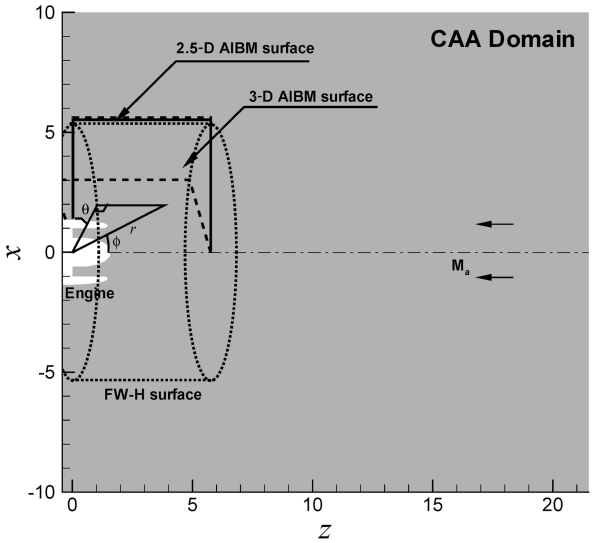

Fig. 7 Schematic diagram of acoustic radiation through an axisymmetric duct intake.

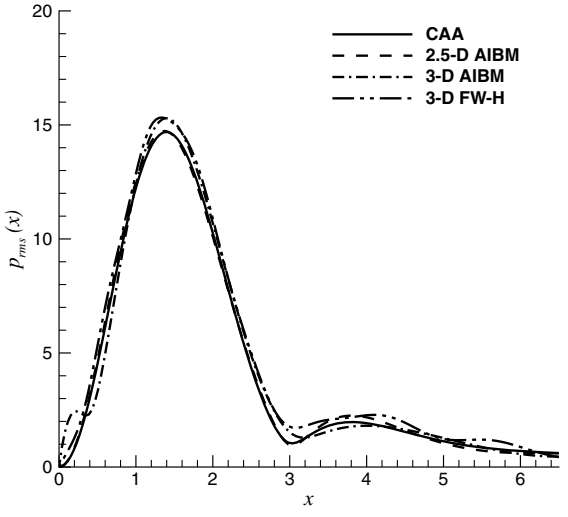

Fig. 8 A comparison of the directivity along the x direction with $z =$ 6.5 m and $y = 0$ for the duct mode of $m = 2$ and $n = 1$.

the angular frequency of 4804.52 Hz is considered. The azimuthal and radial modes used in the CAA calculations are $(m, n) = (2, 1)$, (3, 1), and (4, 1).

The FW–H integral method is the most commonly used method for the far-field acoustic prediction. The method is based on the Navier–Stokes equations and therefore is valid in both the near field and the far field. The AIBM, on the other hand, is based on the linearized Euler's equations and developed for the effective prediction of the far-field acoustic radiation. To show the capability and effectiveness of AIBM in a far-field prediction, the method is coupled with CAA methods for the prediction of the acoustic radiation from the duct intake. The results of AIBM are compared with CAA solutions as well as the solution from the FW–H integral method. Because the acoustic wave is radiating in a 3-D configuration, Farassat's 3-D Formulation 1A [14] with the quadruple term neglected was used in the FW–H integral method. The FW–H surface is depicted in Fig. 7, and the input surface used for AIBM is 1/9 of the FW–H surface, with θ from 0 to 40 deg. The input acoustic data are provided by CAA solutions, and the number of grid points used for the input is 57,960 for the FW–H method and 6440 for the AIBM method. The input data consist of the unsteady pressure and its normal derivative to the input surface for AIBM and the unsteady pressure and velocity for FW–H, respectively. Because the mean flow and the duct intake geometry are both axisymmetric, the simplified 2.5-D formulation for AIBM is also used. The input data for 2.5-D AIBM are given on a number of line segments in the plane of $\theta = 0$ (see Fig. 7).

The acoustic pressure is predicted by AIBM, FW–H, and 2.5-D AIBM at 136 grid points in the range of $0 \leq x \leq 6.5$ m with $z = 6.5$ m and $y = 0$. The results from these methods are compared with the CAA solution in Fig. 8. It is shown that the results from both AIBM and FW–H agree reasonably well with the CAA solution. The computation was performed on a personal computer of Pentium ® 4CPU at 3.2 GHz and memory of 1 GB. The computational time for AIBM is closely related to the number of input points and the number of coefficients a_{nm} and b_{nm}. The CPU time will quadruple as the number of input points doubles and be increased by 8 times if the

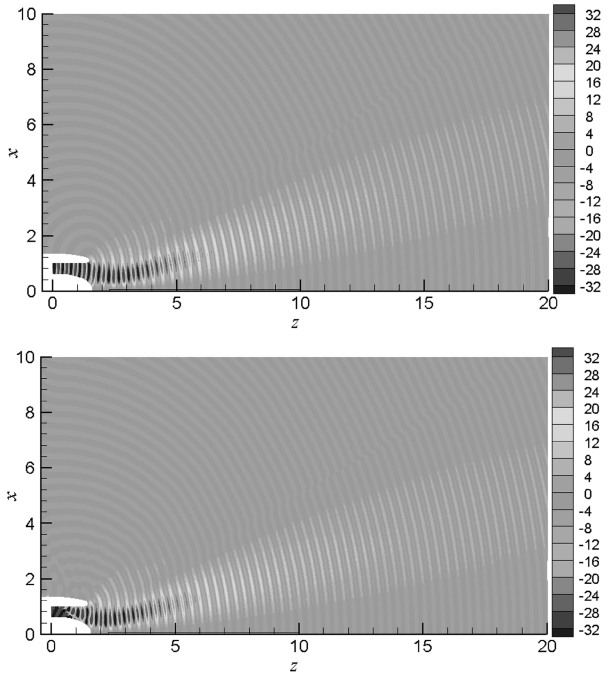

Fig. 9 Instantaneous pressure contours in the plane $\theta = 0$ for the duct mode of $m = 2$ and $n = 1$ showing CAA (top) and AIBM (bottom).

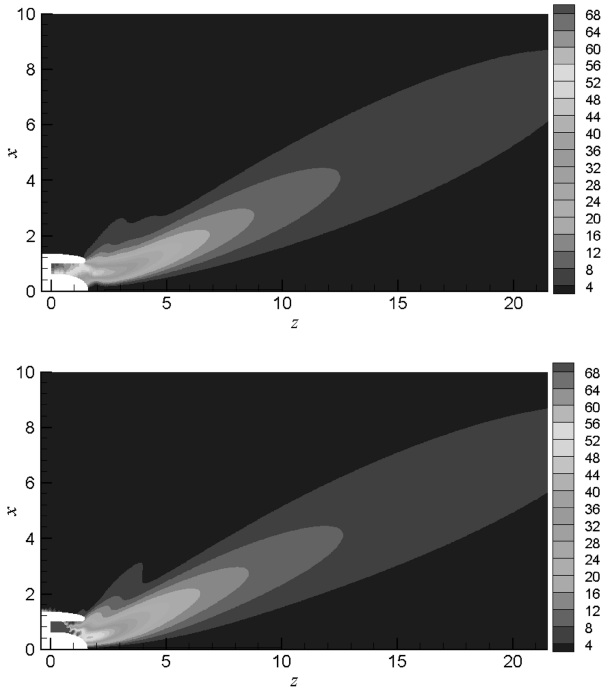

Fig. 10 Pressure amplitude contours in the plane $\theta = 0$ for the duct mode of $m = 3$ and $n = 1$ showing CAA (top) and AIBM (bottom).

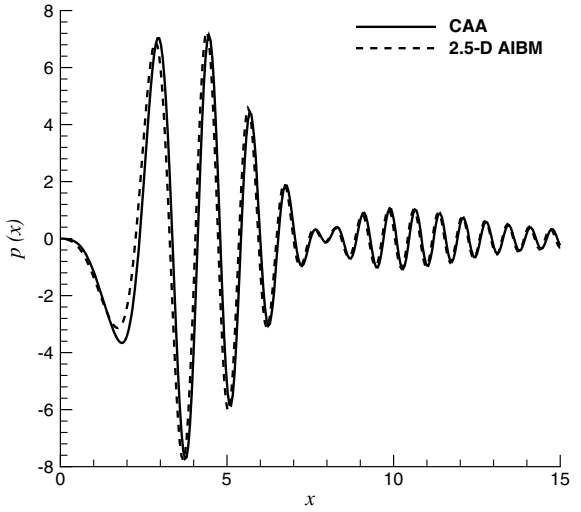

Fig. 11 Comparison of the predicted pressure solution with the CAA solution at $z = 15$ m and $y = 0$ for the duct mode of $m = 2$ and $n = 1$.

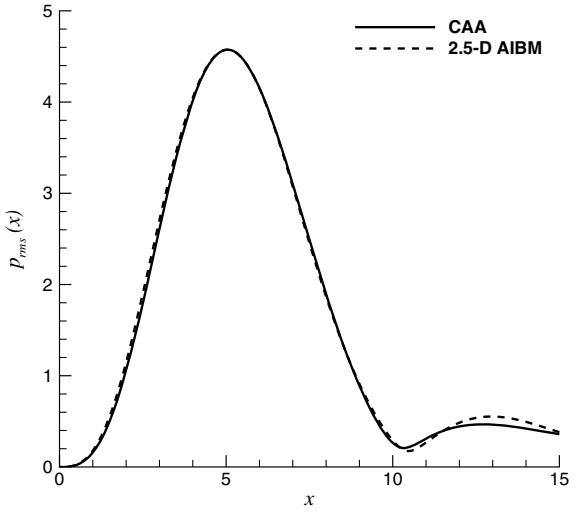

Fig. 12 Comparison of the predicted directivity with the CAA solution at $z = 15$ m and $y = 0$ for the duct mode of $m = 3$ and $n = 1$.

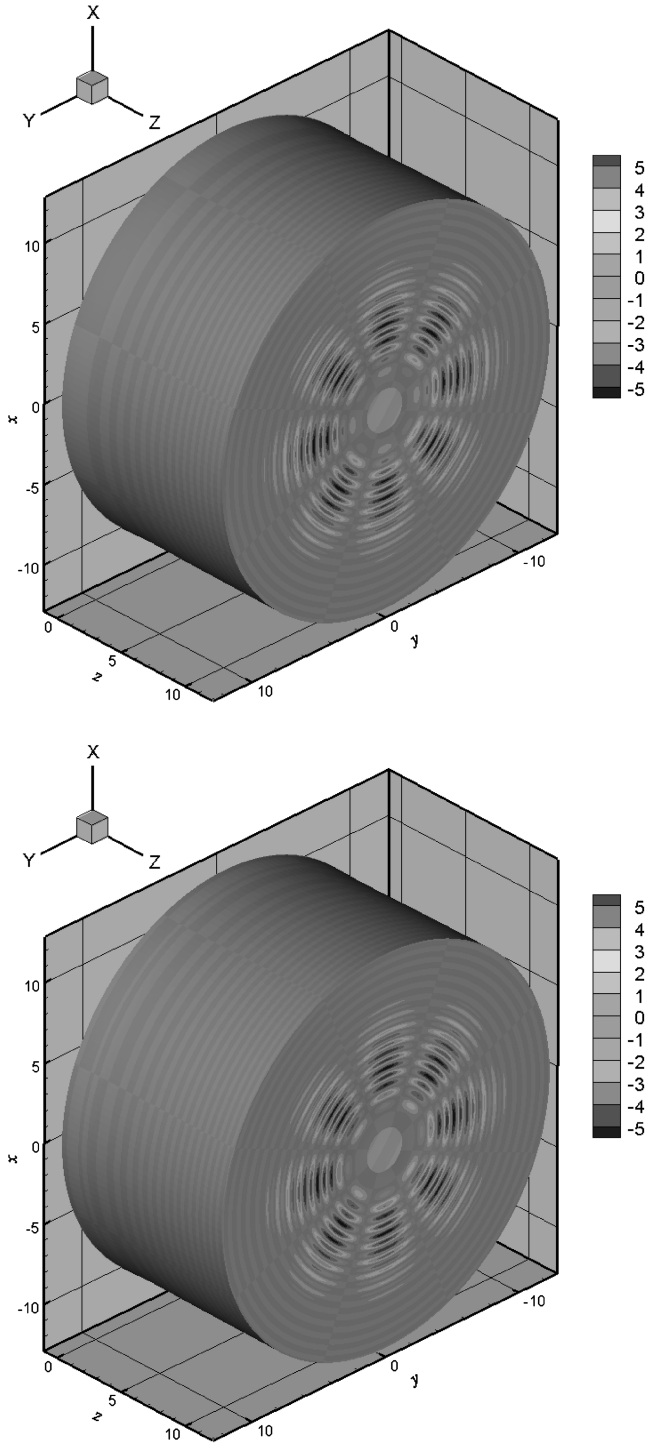

Fig. 13 3-D reconstructed pressure contours for the duct mode of $m = 4$ and $n = 1$ showing CAA (top) and AIBM (bottom).

number of coefficients doubles. For this single frequency radiation problem, the CPU times used for 3-D AIBM and 2.5-D AIBM are 5 min and 4 s, respectively. The total CPU time for FW–H is 16 h. However, the time-domain formulation of FW–H is used, and 64 time increments were considered in the period. The equivalent CPU time for FW–H is 15 min if the frequency-domain formulation of FW–H would be considered. Furthermore, in AIBM the acoustic pressure in a radiated field is calculated analytically after the coefficients of the basis functions are determined. In FW–H, on the other hand, the surface integration has to be carried out for each far-field location. Therefore, AIBM is much more efficient than FW–H and can lead to a significant CPU time reduction if the entire acoustic far field shown in Fig. 7 is to be determined. It is also noted from Fig. 8 that the solution by 2.5-D AIBM agrees very well with the CAA solution. The better agreement can be attributed to a relatively more complete input surface.

Because the problem considered here is axisymmetric, in the following studies, the radiated acoustic field is calculated based on the 2.5-D AIBM formulation. The instantaneous pressure contours and the pressure amplitude contours obtained by 2.5-D AIBM are compared with the CAA solutions in Figs. 9 and 10 for the duct modes of (2, 1) and (3, 1), respectively. In addition, the quantitative comparisons of the acoustic pressure for the (2, 1) mode and the directivity for the (3, 1) mode are given in Figs. 11 and 12, respectively. The results shown in these figures clearly demonstrate the effectiveness of AIBM for the prediction of far-field acoustic radiation. It is noted that the solution inside and in the vicinity of intake, although not valid, was kept in the contour plots for convenience. In addition, the input acoustic data for AIBM should be given away from aerodynamic noise sources in order to guarantee the accuracy of the predicted acoustic solution in radiated fields. The reconstructed 3-D instantaneous pressure contours by AIBM are compared with the CAA solution in Fig. 13 for the duct mode of (4, 1). The capability and the overall effectiveness of AIBM for aeroacoustic applications are demonstrated by the example.

IV. Conclusions

The AIBM for the reconstruction and prediction of far-field acoustic radiation is successfully extended to a three-dimensional configuration. The extended AIBM is applied to various acoustic propagation and radiation problems, such as the propagation of multiple sources, the scattering of a time-dependent acoustic source, and the propagation and radiation of duct acoustic modes from an axisymmetric duct intake. The predicted acoustic fields by AIBM for all the cases agree very well with the respective analytical solutions or the CAA and the FW–H solutions. The main advantages of AIBM over the FW–H integral method are its efficiency and capability of accurately predicting the far-field acoustic propagation based on the acoustic input from an open surface in the radiated field. The disadvantage of AIBM is that the method is effective only when the input data are given in a radiated field away from acoustic sources. In a summary, AIBM provides an effective alternative for the far-field acoustic prediction of practical aeroacoustic problems.

Acknowledgments

Chao Yu would like to acknowledge the financial support from the Technical University of Berlin. Xiaodong Li is supported by grants from the 973 program 2007CB714604 and the 111 project-B07009 of China. We would like to thank Dakai Lin of Beihang University for his assistance on computational aeroacoustics solutions for the duct intake problem.

References

[1] Lighthill, M. J., "On Sound Generated Aerodynamically, I: General Theory," *Proceedings of the Royal Society of London A*, Vol. 211, No. 1107, 1952, pp. 564–587. doi:10.1098/rspa.1952.0060

[2] Farassat, F., and Myers, M. K., "Extension of Kirchhoff's Formula to Radiation from Moving Surfaces," *Journal of Sound and Vibration*, Vol. 123, No. 3, 1988, pp. 451–461. doi:10.1016/S0022-460X(88)80162-7

[3] Ffowcs Williams, J. E., and Hawkings, D. L., "Sound Generated by Turbulence and Surfaces in Arbitrary Motion," *Philosophical Transactions of the Royal Society*, Vol. 264, No. 1151, 1969, pp. 321–342. doi:10.1098/rsta.1969.0031

[4] Yu, C., Zhou, Z., and Zhuang, M., "An Acoustic Intensity-Based Method for Reconstruction of Radiated Fields," *Journal of the Acoustical Society of America*, Vol. 123, No. 4, 2008, pp. 1892–1901. doi:10.1121/1.2875046

[5] Yu, C., Zhou, Z., and Zhuang, M., "An Acoustic Intensity-Based Inverse Method for Sound Propagations in Uniform Flows," AIAA Paper 2007-3563, 2007.

[6] Jerison, D., and Kenig, C. E., "Unique Continuation and Absence of Positive Eigenvalue for Schrodinger Operators," *Annals of*

Mathematics, Vol. 121, No. 3, 1985, pp. 463–494.
doi:10.2307/1971205

[7] Dowling, A. P., and Ffowcs Williams, J. E., *Sound and Sources of Sound*, Cambridge Univ. Press, Cambridge, England, UK, 1983.

[8] Zhuang, M., and Chen, R., "Applications of High-Order Optimized Upwind Schemes for Computational Aeroacoustics," *AIAA Journal*, Vol. 40, No. 3, 2002, pp. 443–449.
doi:10.2514/2.1694

[9] Morris, P. J., "Scattering of Sound from a Spatially Distributed, Spherically Symmetric Source by a Sphere," *Journal of the Acoustical Society of America*, Vol. 98, No. 6, 1995, pp. 3536–3539.
doi:10.1121/1.413786

[10] Ozyoruk, Y., and Long, L. N., "Computation of Sound Radiating from Engine Inlet," *AIAA Journal*, Vol. 34, No. 5, 1996, pp. 894–901.
doi:10.2514/3.13165

[11] Li, X. D., Schemel, C., Michel, U., and Thiele, F., "Azimuthal Sound Mode Propagation in Axisymmetric Duct Flows," *AIAA Journal*, Vol. 42, No. 10, 2004, pp. 2019–2027.
doi:10.2514/1.11952

[12] Li, X. D., Schoenwald, N., Yan, J., and Thiele, F., "A Numerical Study on the Acoustic Radiation from a Scarfed Intake," AIAA Paper 2003-3245, 2003.

[13] Li, X. D., Duan, C., and Yu, C., "On the Matching Technology Between the 3-D FW–H Equation and CAA Numerical Simulations," *Journal of Engineering Thermophysics*, Vol. 26, No. 1, 2005, pp. 51–54 (in Chinese).

[14] Farassat, F., "Derivation of Formulations 1 and 1A of Farassat," NASA Technical Rept. NASA/TM-2007-214853, March 2007.

J. Wei
Associate Editor